Proceedings World Geothermal Congress 2020+1
Reykjavik, Iceland, April - October 2021

Electrical resistivity applied to understand the geothermal fluid flow pathway and define borehole targets in a geothermal area, Liquiñe, Chile

Nicolás Pérez-Estay, Pablo Valdenegro, Tomás Roquer, Eduardo Molina, Gloria Arancibia, Diego Morata

Plaza Ercilla 803, Santiago, Chile

nnperez@uc.cl

Keywords: Thermal springs, Hot-springs, Electrical resistivity tomography, Low-enthalpy geothermal prospection, Southern Andes, Archie's law, Borehole targets.

ABSTRACT

Low-enthalpy geothermal production processes can be developed using the available resource of thermal springs. But occasionally of higher volumetric flow rates and/or temperatures are required (e.g. long hot-fluid transportation due to space limitations, increasing the heat demand to improve production, among others). For that reason, understanding the geometry and spatial distribution of shallow geothermal systems (~30 meters) can be useful to define the potential borehole drilling targets, and finally, increase the volumetric flow and/or the temperature of the fluid. We performed 4 Electrical Resistivity Tomographies (ERT) and applied Archie's law for this purpose. From the ERT profiles, three electrical resistivity domains could be distinguished: i) a high resistivity domain (1000-6000 Ohm-m), interpreted as a pristine or low fractured rock. ii) a horizontal low-resistivity domain (1-300 Ohm-m) in the upper 5-10 meters, which is interpreted as soil and\or unconsolidated sediments partially saturated with thermal water. Finally, iii) slightly vertical bodies with low resistivities (30-300 Ohm-m) immersed in the high resistivity domain. These are interpreted as fractured rock or damage zone related with the surrounding fault systems. Considering our interpretations, two borehole targets are defined: the horizontal low-resistivity domain and the vertical low-resistivity domain; where the last one is suggested as the best target due to pressure and temperature conditions expected in an upwelling damage zone.

1. INTRODUCTION

Several production processes require low-enthalpy geothermal energy with temperatures above 50°C, such as fruit dehydration (e.g., Kostoglou et al., 2010) or milk pasteurization (e.g., Lund & Falls, 1997; Yadav & Sircar, 2018). Thus, the thermal springs are used worldwide to develop these processes (e.g., Jubaedah et al., 2015; Thayer et al., 1989). First-order parameters necessary for engineering design are the volumetric flow rate, pressure and temperature of the fluid, the spatial distribution of the network, efficiency of the system, and the energy demand, among others (e.g., Rees, 2016). Thus, in the case of geothermic from thermal springs, the capacity for developing low-enthalpy processes it is restricted by the volumetric flow rate, temperature, and pressure of each spring. In some cases, the springs do not satisfy the engineering-design necessities. For example, the lack of space requires hot-fluid transportation along with longer distances increasing its energy losses; or the necessity of increasing the production requires more heat energy. For that reason, defining the shallow geometry of a geothermal system (*e.g.,* the geometry of conduits/barriers for fluid flow) allows the discrimination of potential borehole targets, from which the energetic potential of the geothermal system and engineering requirements can be assessed.

Geophysicists have made many efforts to understand thermal spring geometries. Electrical resistivity tomography (ERT) and Self-potential (SP) arise as the most used geophysical methods in the last decades (e.g., Revil & Jardani 2013; Revil et al. 2015; Richards et al. 2010; Fikos et al. 2012; Tripp et al. 1978; Chabaane et al. 2017). These methods are the most used because of the electrical properties of the medium are notoriously affected by the fluid presence (e.g., Revil & Jardani 2013) or temperature changes (e.g., Dakhnov, 1962). From another perspective, hydrogeology has developed and used Archie's Law to understand the bulk electrical resistivity of a porous medium filling with a conductivity fluid (Archie, 1942), mainly for prospection and extraction of hydrocarbons. The aim of this work is the combination of the ERT method, with Archie's law calibrated with in-situ thermal water conductivity, to understand the shallower geometrical structure (~30 m depth) of an active geothermal system placed in Liquiñe, southern Andes, Chile. Finally, we discuss possible borehole targets to improve the temperature and/or volumetric fluid flow near to a thermal spring.

The selected Liquiñe area is located in an intra-volcanic-arc zone with several geothermal manifestations, and thus, it represents an interesting study-case to understand the thermal water circulation in the shallower segment of a geothermal system. At least six thermal spring sites have been recognized in Liquiñe (see Fig. 1). We analyze and present here only one specific thermal spring site, named *Hipólito Muñoz* because it has several thermal springs with the highest temperature reached (>60 °C) in the Liquiñe area.

2. GEOLOGICAL FRAMEWORK

The Liquiñe area is located in the Southern Volcanic Zone (SVZ), Chile, at ~40°S latitude (Fig. 1a). Here, at least fifteen surface thermal springs occur, with measured surficial temperatures ranging between 40 and 85°C (Lara and Moreno, 2004; Espinoza, 2017). Thermal springs are spatially associated with two different groups of faults. 1) the Liquiñe-Ofqui Fault System (LOFS), which is composed of dextral, dextral-reverse, and dextral-normal NS-to-NE striking faults. 2) the Andean Transverse Faults (ATF), that represent sinistral and sinistral-reverse NW-to-WNW striking faults (e.g., Perez-Flores et al. 2016; Tardani et al. 2016; Cembrano and Lara 2009). In the study area, five geological units were recognized, which constitute the host lithologies for occurring geothermal systems (Fig. 1b) (Cembrano et al., 2000; Lara and Moreno, 2004; Sánchez et al., 2013). These are crystalline granitic to dioritic rocks (from Jurassic to Cretaceous and Miocene emplacement ages); fractured granitoid rocks close to faults (separated by less than 1 km); crystalline metamorphic rocks (Paleozoic age); volcanic rocks (from Pleistocene to Holocene ages); and unconsolidated sedimentary deposits (fluvial, colluvial, glacial and ash Quaternary deposits).

From the different thermal spring sites identified, we focus in the *Hipólito Muñoz* (Fig.1b-c). In the selected site, we found 13 thermal springs upwelling from fluvial or colluvial deposits. Thermal springs are concentrated around a recognized N71°W-trending geomorphological lineament, attributable to the ATF. This site is located on the northern slope of the valley.

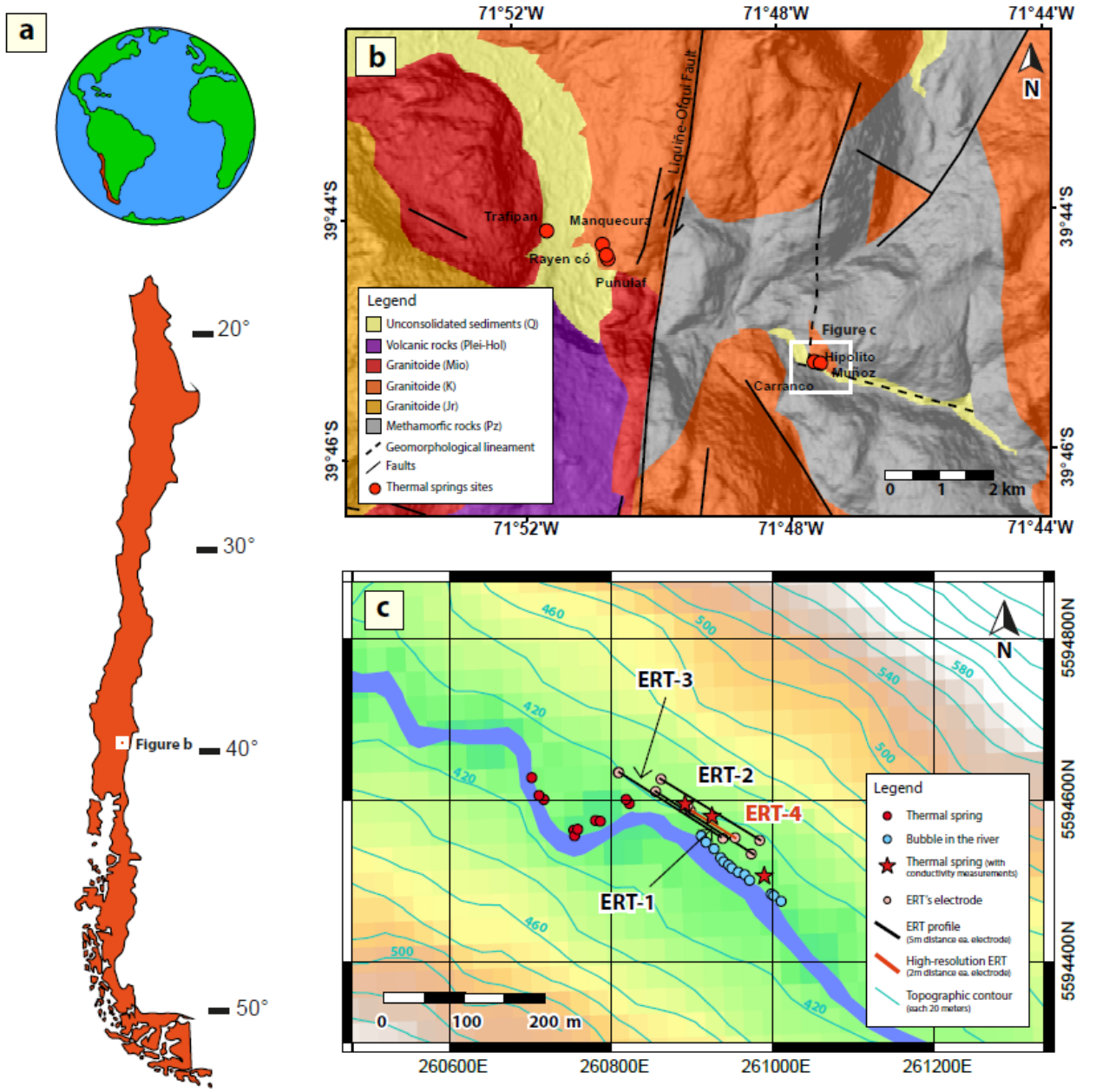

Figure 1: Geology map of the study area. a) World-scale location. b) Geological map of the Liquiñe area, modified after Cembrano et al. (2000) and Lara and Moreno (2004). c) Hipólito Muñoz thermal site showing the electrical tomography profiles and thermal springs.

3. METHODOLOGY

We performed four electrical resistivity tomography measurements above two thermal springs (see Fig. 1c). These electrical tomographies were carried out with the *Tigre* equipment *(Allied Associates, U.K.),* equipped with 32 electrodes every 5 meters. All the tomography profiles were measured with ~N65°W trending azimuth, mainly because of restricted terrain access due to dense forest cover and the narrow valley. Three of these electrical tomographies were done with the maximum electrode spacing (5 meters), giving a total tomography length of 155 meters. Additionally, to acquire a high-resolution tomography close to one thermal spring, ERT04 was carried out with an electrode spacing of 2 meters, giving a tomography length of 62 meters. All the tomographies were done with a Dipole-Dipole array configuration. For details of this method, see Telford et al. (1990, Chapt. 8). To obtain the final electrical tomography profiles, we carried out an inversion with *ZondRes2d* software. A precise topography is required to obtain accurate inversion results; thus, we used a *Trimble R4* DGPS to locate the electrodes, obtaining a mean position error of 0.25 meters.

Archie's law correlates the electrical conductivity of a porous medium with the electrical conductivity of the filling fluid according to the equation (1) (e.g., Archie, 1942; Glover, 2016):

$$\sigma_b = c\ \sigma_f \theta^m \quad (1)$$

Where σ_b is the bulk or medium electrical conductivity, σ_f is the filling fluid's electrical conductivity, θ is the medium porosity, and parameters c and m are unidimensional empirical parameters. This law assumes that the electrical conductivity of grains is extremely lower than the fluid. Hence, current paths move through the fluid and the bulk electrical conductivity only depends on the fluid proprieties and its volume (see right side of equation 1). However, this assumption is not true in clays soils because of its cation exchange capacity (e.g., Revil & Jardani, 2013). To constrain *in-situ* fluid's electrical conductivity, we measured six thermal springs (see Table 1 and Fig. 1-c) by means of a *HI 9811-5* multiparameter *(Hanna instruments, U.S.A)*. We use the mean value of the six samples to define σ_f. Note that all the samples have two temperatures (in Table 1) because the *HI 9811-5* multiparameter has a measure-temperature-range below 65°C. Thus, we measured the electrical conductivity with the samples waiting 1 minute in a geochemical-standard sterile bottle. Additionally, we measured the temperature of the thermal spring with a thermocouple. Parameters c and m were obtained from the bibliography (Friedman, 2005; Shah & Singh, 2005). Finally, the porosity is an unconstrained parameter due to the lack of a borehole. Considering this, we decided to analyze the possible porosity variability defining four cases, with porosities of 20%, 30%, 40%, and 50%. Additionally, note that the electrical resistivity of some medium (ρ_m), or fluids (ρ_f) is the inverse of the electrical conductivity ($\sigma_{f,m}$), as evidence equation (2). To analyze the ERT results, we will focus on the electrical resistivities values instead of the conductivity.

$$\rho_{f,m} = \frac{1}{\sigma_{f,m}} \quad (2)$$

4. RESULTS

4.1 Electrical resistivity tomographies

The results of the electrical tomographies inversion are shown in Figure 2. Electrical resistivity values range from 1 to 6000 Ohm-m, and the root mean square errors (RMS) of the different profiles are 4.0%, 2.6%, 7.7%, and 3.1%, respectively. All profiles show three different electrical resistivity domains.

First, a widespread high-resistivity domain with electrical resistivity ranging between 1000 and 6000 Ohm-m.

Second, horizontal low-resistivity bodies in the shallower part of the profiles, specifically between the surface and the upper 10 m depth. For example, in the high-resolution profile (ERT-4), two slightly low-resistivity horizontal bodies are observed within the upper 5 meters (Fig. 2d). In addition, the ERT-1 tomography has one horizontal body within the upper 5 meters (Fig. 2a). In both cases, these horizontal bodies are not continuous along with the profile. Conversely, ERT03 has the best-exposed horizontal body along with the entire profile (Fig. 2c). These horizontal bodies have electrical resistivities ranging between 1 and 300 Ohm-m, with values below 10 Ohm-m presented in circular shapes (see grey circular shapes in ERT-1 and ERT-03, Fig. 2).

Third, the last electrical domain is composed of low-resistivity bodies with nearly vertical shapes between the bottom of each profile and the upper 5-10 meters below the surface. For example, in Figure 2-c, three different sub-vertical low-resistivity bodies can be observed (electrical resistivity from 10 to 100 Ohm-m). In the other profiles, sub-vertical shapes also are observable (e.g.. at 40 and 80 meters of horizontal distance in profile ERT-02, Fig. 2b). Generally, for these low-resistivity bodies, electrical resistivity ranges from 10 to 300 Ohm-m. These bodies have no more than 15 meters wide and are present in every segment of the study area, which makes them observable in all the profiles.

4.2 Archie's law application

From the electrical resistivity of the samples (see Table 1), we can see the obtained mean electrical resistivity of the thermal water in ρ_f = 19.5 Ohm-m. Differences between the thermal spring temperature and the resistivity-measured temperature are around 10-20°C (columns 2 and 3 in Table 1). This yields some differences in estimated underground thermal water electrical resistivity since electrical resistivity depends on the temperature (e.g. Dakhnov, 1962). However, samples Hipo-1, Hipo-2, and Hipo-3 have the same electrical resistivity of 19 Ohm-m but 10°C of difference in temperature. Thus, the temperature may be not the first-order parameter affecting the fluid's electrical resistivity. Hence, we have some errors related to the variability in the electrical resistivity of the thermal waters, that in our case, range from 19 to 21 Ohm-m, according to the six samples of Table 1. For our propose, this small error-range will be despised and we will use the mean electrical resistivity ρ_f = 19.5 Ohm-m.

Table 1. Results of the electrical resistivity measurements in different thermal springs.

Sample name	Temperature of spring [°C]	Temperature of measure [°C] *	Electrical conductivity [µS/cm]	Electrical resistivity [Ohm-m]
Hipo-1	80	61	540	19
Hipo-1b	80	54	490	20
Hipo-2	69	50	540	19
Hipo-2b	69	49	470	21
Hipo-3	77	60	540	19
Hipo-3b	77	59	500	20

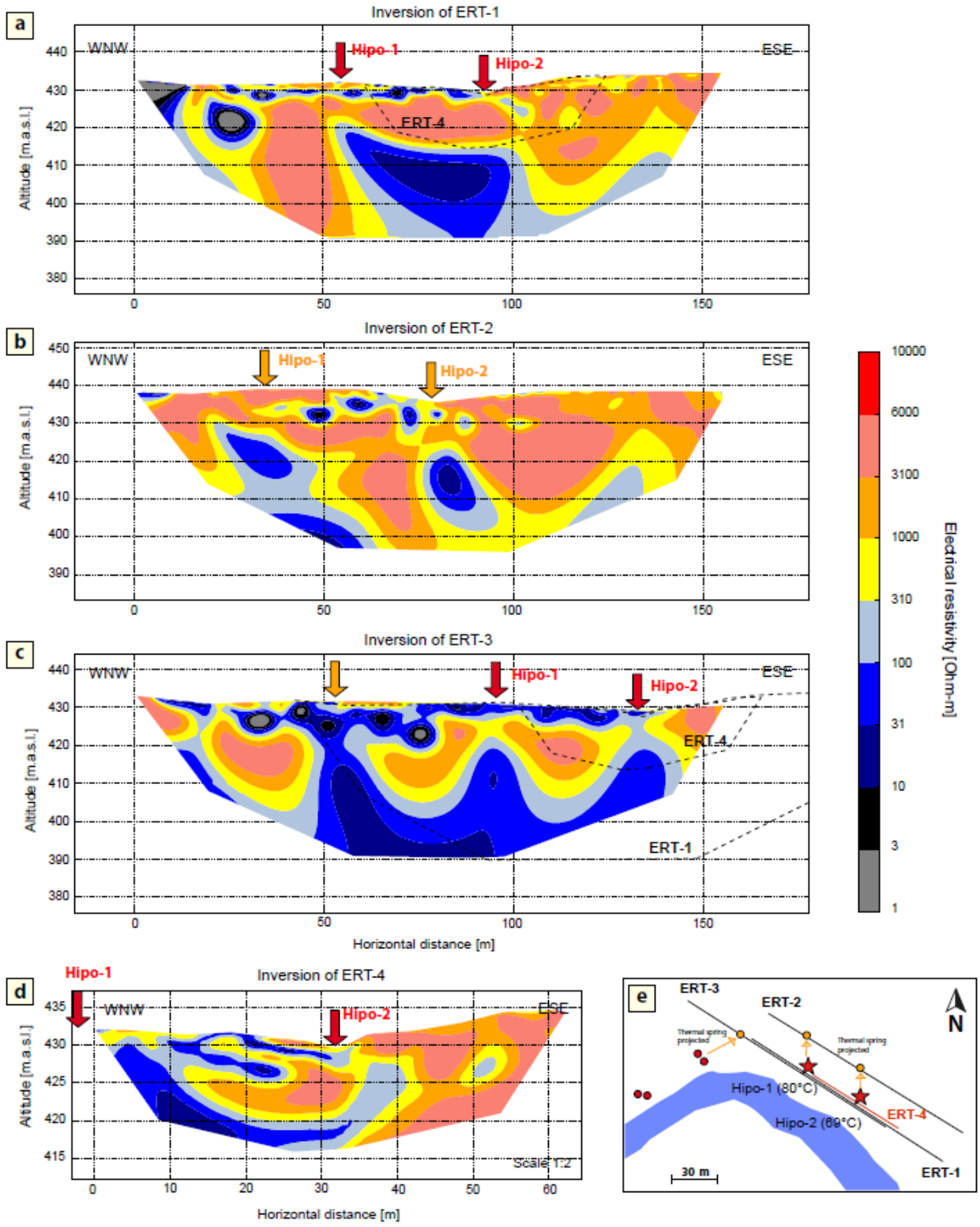

Figure 2: Electrical resistivity tomographies (ERT) results. ERT01 (a), ERT02 (b), and ERT03 (c) have the same scale, without vertical exaggeration. d) ERT-4 electrical tomography results, with scale 1:2 respect to the other profiles, but without vertical exaggeration. All the profile has the same electrical resistivity scale. Red arrows show the real position of the thermal springs over the profile, and orange arrows symbolize projected nearby spring to the profile, as it can be observed in the detailed map (e). e) Close up map whit the location of the different profiles in black lines; the thermal springs in red circles, and the projected spring to the profiles in orange circles; the river Ranintulelfu in blue.

Empirical parameters c and m were obtained from Shah and Singh (2005), where soils with different grain mineralogical composition were analyzed. In soils without clays (in the size meaning of the word, d < 0.002 mm), the authors define the parameters c=1.45 and m=1.25. Considering four cases with different porosity values, we can define a range for the bulk-electrical resistivity of the medium saturated with thermal water (Table 2). Then, it is expected that the porous medium saturated with thermal water would have an electrical resistivity ranging between 32 and 100 Ohm-m, estimated from equation 1. This range is hereafter referred to as Archie's law range.

Table 2. Different cases to define an electrical resistivity range for soil saturated with thermal water.

	Case 1	Case 2	Case 3	Case 4
Water resistivity [Ohm-m]	19.5	19.5	19.5	19.5
Porosity	0.2	0.3	0.4	0.5
Parameter c	1.45	1.45	1.45	1.45
Parameter m	1.25	1.25	1.25	1.25
Medium resistivity saturated with hot water [Ohm-m]	**100.5**	**60.5**	**42.3**	**32.0**

5. DISCUSSIONS AND INTERPRETATIONS

Understanding the geological meaning of the electrical tomographies is necessary to define precise borehole targets. For this purpose, we will discuss first the geological interpretation of the ERTs, and then we will discuss the best borehole targets.

5.1 Understanding the shallowest geometry of this geothermal system from the ERTs

The first lithoelectrical domain has a high resistivity range (1000-6000 Ohm-m), which represents typical values for pristine plutonic and/or metamorphic rocks (e.g., Loke, 2004; Telford et al., 1990). The narrow valley (< 200-300 m width, Fig. 1-b) and the high slope angles in the area (see elevation contour in Fig. 1-c) do not allow the formation of a deep sedimentary basin or fluvial terraces. Thus, the rock basement should be measurable within the upper 30 me of the profile. The spatial distribution of the high-resistivity domain is in good agreement with this geological observation (Figs. 1c and 2). The widespread domain is observed in the deeper sections of the profiles, mostly between the bottom of profiles and the upper 5 m, with the exception of the profile ERT02, where the widespread high-resistivity domain is observed from the bottom to the surface. According to the geological map (Fig. 1b), in the northern slope of the valley where measurements were performed, Cretaceous granitoids constitute potential rocks. Electrical resistivities measured in granites at different geological contexts have similar resistivity range that this high-resistivity domain. For instance, wet granite has a mean electrical resistivity of 4400 Ohm-m (Telford et al., 1990), and the Westerly granite in (USA) has a resistivity ranging between 4000 and 20 000 Ohm-m (Duba et al., 1978). In that sense, the spatial distribution and the electrical resistivity range, suggests that the high resistivity domains likely correspond to pristine or low fractured granitic rocks.

The second domain is a horizontal volume, always occurring in the shallowest portion of the electrical profiles (<10 m depth). The horizontal shape suggests that this unit corresponds to soil or unconsolidated sediments deposited in layers. This is consistent with field observations, where exposed volumes of soil with 1 to 2 meters of thickness can be observed close to the profiles (Fig 3d). Thus, we interpret the second lithoelectrical domain as soil and/or unconsolidated deposits. Resistivity values of this domain range between 1 and 300 Ohm-m, which is in good agreement with expected resistivity values for sedimentary deposits (Loke, 2004; Telford et al., 1990).

Archie's law indicates that a porous medium saturated with thermal water may have resistivities between 32 and 100 Ohm-m. Hence, resistivities between 100 and 300 Ohm-m of this domain may represent the absence or negligible presence of thermal water. Conversely, resistivities between 32 and 100 Ohm-m could represent unconsolidated sediments saturated with thermal waters. This range is present all around the horizontal bodies and is common in the vicinity of thermal springs. The spatial association of thermal spring with the 32-100 Ohm-m values suggests that hot water might be found in this electrical resistivity range. Additionally, low-resistivity values between 1 and 10 Ohm-m are out of Archie's laws range by roughly one order of magnitude. Hence, these low values need another explanation, which could be: 1) a highly porous sedimentary layer filled with thermal water; 2) highly conductive thermal waters (σ_f); or 3) clay precipitation.

The first scenario is not realistic, because even with 90% of porosity (unlikely state), by applying Archie's law, the bulk electrical resistivity would be 15 Ohm-m. The second scenario needs an increase in σ_f in at least 400% to obtain a bulk electrical resistivity (ρ_b) of 8 Ohm-m in case 4 of Table 1 (0.5 of porosity, the most favorable case), applying equation 1 and 2. To obtain values of 1 Ohm-m, an increase of σ_f in 2000% is necessary in the same favorable-boundary case of 0.5 porosity. The high increase of 400 to 2000% of the electrical conductivity in thermal water is difficult to explain, and the measured variability of this parameter ranges between is 470 and 540 µS/cm (see Table 1) suggesting only 15 % of the variability. The third option is more plausible, due to mineral deposition observed in the surface hot-water flows (e.g., Fig. 3c). Additionally, clay presence may considerably lower the electrical resistivity of the medium because of the cation exchange capacity (CEC) of clays (e.g., Revil & Jardani, 2013).

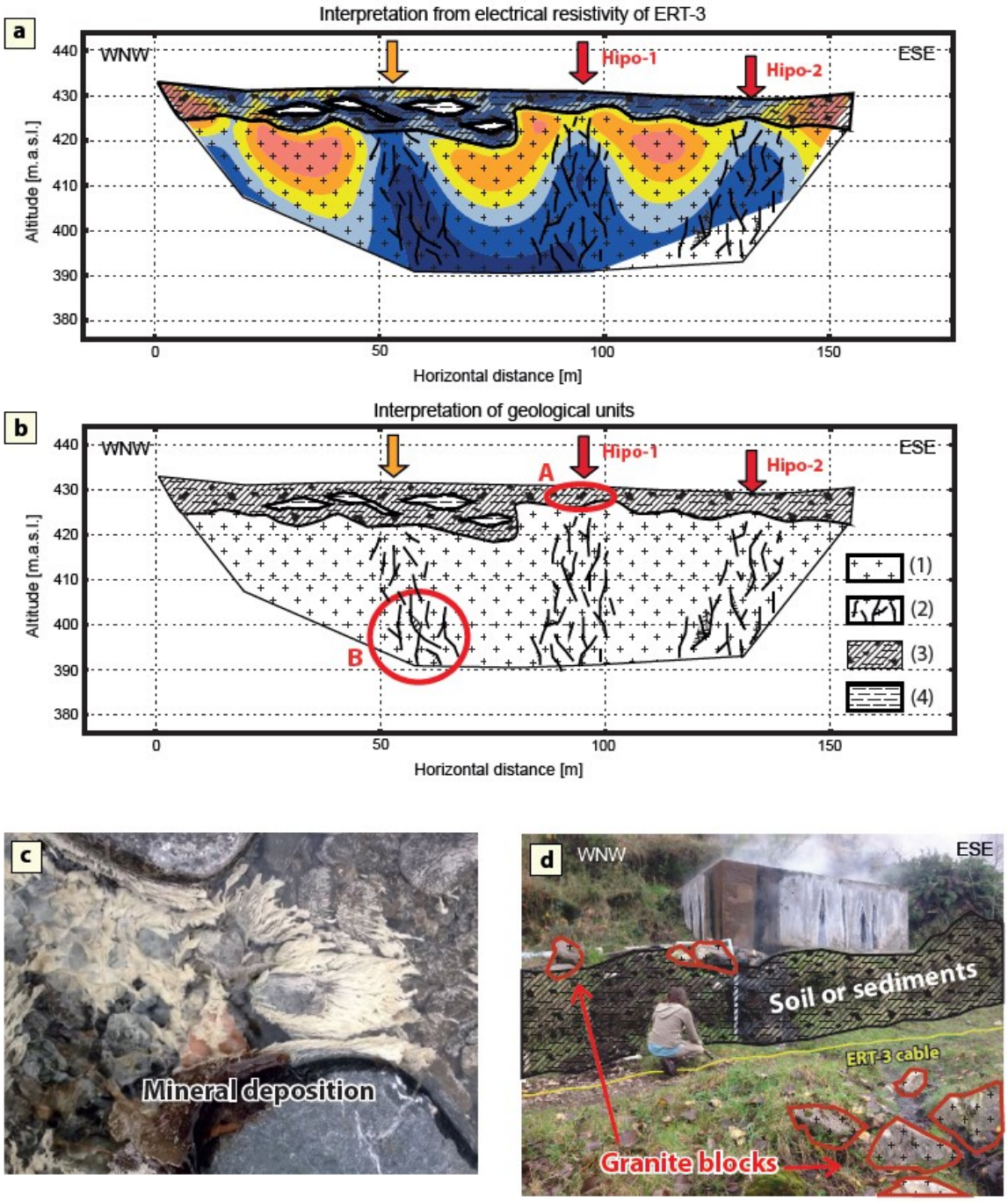

Figure 3: Interpretation of the electrical resistivity tomography ERT-3. a) geological interpretation with the electrical resistivity below. Thermal springs in a) and b) are de same as Figure 2-c. b) geological interpretation alone, with red ellipses showing both possible borehole targets. The units are: 1) low fracture granitic rock; 2) highly fractured granitic rock; 3) Unconsolidated sediments with several granite blocks; 4) Clay lenses associated with the thermal water flows. c) Plan view photography evidencing white minerals disposition in hot water flows on the surface. d) Soil or unconsolidated sediments close to the ERT-3 deployed, with granite block of 20 to 60 centimeters.

Finally, the electrical resistivity of clays ranges in the available literature varies from 1 to 100 Ohm-m (Loke, 2004; Telford et al., 1990), suggesting that the clay presence is the most acceptable interpretation. Thus, we interpret this horizontal low-resistivity domain as segments of unconsolidated sediments partially saturated with thermal water, and with clay lenses close to some hot springs (see Fig. 3b).

The third domain with electrical resistivities ranging between 10 and 300 Ohm-m is immersed in the first high-resistivity domain previously interpreted as unfractured/pristine rock. Its slightly vertical shape only allows two explanations: i) sub-vertical dikes host in the granitoid rocks, or ii) fractured granitoid rock related to a fault damage-zone. No dikes were observed in the proximity of the area in the Cretaceous granite and/or the Paleozoic metamorphic gneiss. Thus, it is difficult to expect the unexposed dikes to be located just below the hot-spring. The second option arises as the most plausible, as the presence of thermal water around 60-80°C at surface level implies deep hydrothermal interaction between a heat source and the observed fluid. In this context, fractured rocks represent high permeability domains, a condition needed to allow the hot-water ascent. Fractured rocks spatially correlated with

thermal spring have been documented by other authors (e.g., Perez-Flores et al., 2016; Tardani et al., 2016). Additionally, the electrical resistivity range of this domain is mostly contained in Archie's law range. Therefore, the resistivity values are coherent with the thermal water presence. Furthermore, all these sub-vertical low-resistivity bodies are below a thermal spring or springs projections (see Fig. 2-a, b, c and d). Therefore, because of the electrical resistivity range similarity with Archie's range and the sub-vertical shape immersed in the rock, we interpret this domain as vertical fractured rock saturated with thermal water. Note that the widespread occurrence of theses sub-vertical bodies could explain the widespread thermal spring of the site observed in Figure 1-c.

5.2 Borehole targets definition

Finally, borehole targets are defined within the interpreted geological units saturated with thermal water, especially the horizontal and the sub-vertical low-resistivity bodies.

The first one, interpreted as soil or unconsolidated sediments, appears as a target. Nevertheless, this unit has some segments with electrical resistivities up to Archie's law range, suggesting that it is not completely saturated. Also, as previously discussed, extremely low-values between 1 and 10 Ohm-m suggest clays lenses. Borehole targets should avoid clays and unsaturated soils, as clays correspond to low-permeability domains (e.g., Revil & Jardani, 2013), and unsaturated soils do not ensure an increase in the volumetric flow rate. Consequently, we suggest the red ellipse A (Figure 3-b) as an appropriate drilling target, due to its proximity to a thermal spring and a resistivity range between 30 and 100 Ohm-m (Archie's law range).

The secondary targets (ellipse B in Figure 3-b) could be the sub-vertical low-resistivity bodies, named as the third unit in the results and discussion above. According to our interpretation, they represent fractured rocks saturated with thermal water. Following our interpretations, the pressure of this target must be greater than the horizontal superficial sediments, considering the rock thickness and soil column. Hence, greater pressure may suggest better conditions to increase the volumetric flow rate. Additionally, a deeper location with respect to target A may represent an equal or higher water temperature assuming a one-dimensional vertical heat advection regime (e.g., Anibas et al., 2009). Therefore, the possibilities of better pressure and temperature condition make the second target B a better prospect.

6. CONCLUSIONS

Four electrical resistivity tomographies were carried out close to two thermal springs. Additionally, Archie's law was used to define the electrical resistivity range for soil-porous medium saturated with thermal waters. Interpretation of the ERTs combining Archie's law, suggests two different targets to improve the temperature and/or volumetric fluid flow of the thermal emplacement:

1) The first one is the horizontal low-resistivity bodies in the first 5-10 upper meters, where the electrical resistivity range and the spatial association with the thermal springs suggest the thermal water presence.

2) The second one is the sub-vertical low-resistivity bodies present below the thermal springs of ~10 meters width. This was interpreted as fractured rocks saturated with thermal water, and thus, present the best conditions of pressure and temperature to constitute a borehole target.

ACKNOWLEDGMENTS

This work is a contribution to the FONDAP Project #15090013, "Centro de Excelencia en Geotermia de los Andes" (CEGA) and to the regional government of the Los Rios Region for partially funding this work with the project FIC code BIP 30486383-0. Part of the fieldwork was carried out with financial support from the FONDECYT project #1180167. Tomás Roquer acknowledges financial support from CONICYT PhD grant #21171178. Authors thank Diego Aravena, Camila Aravena and María Paz Quercia for fieldwork, and Juan Daniel Riquelme and his family for allowing us access to the Hipólito Muñoz thermal complex.

REFERENCES

Anibas, C., Fleckenstein, J., Volze, N., Buis, K., Verhoeven, R., Meire, P., & Batelaan, O.: Transient or steady-state? Using vertical temperature profiles to quantify groundwater–surface water exchange. *Hydrological Processes*, **23**, (2009), 2165–2177. https://doi.org/10.1002/hyp.7289

Archie, G. E.: The Electrical Resistivity Log as an Aid in Determining Some Reservoir Characteristics. *Transactions of American Institute of Mining Metallurgical Engineers*, **146**, (1942), 54–62. https://doi.org/10.2118/942054-G

Cembrano, J., Schermer, E., Lavenu, A., and Sanhueza, A.: Contrasting Nature of Deformation along an Intra-Arc Shear Zone, the Liquiñe–Ofqui Fault Zone, Southern Chilean Andes. *Tectonophysics,* **319**, (2000): 129–49. https://doi.org/10.1016/S0040-1951(99)00321-2.

Cembrano, J., & Lara, L.: The link between volcanism and tectonics in the southern volcanic zone of the Chilean Andes: A review. *Tectonophysics*, **471**, (2009), 96–113. https://doi.org/10.1016/j.tecto.2009.02.038

Chabaane, A., Redhaounia, B., & Gabtni, H.: Combined application of vertical electrical sounding and 2D electrical resistivity imaging for geothermal groundwater characterization: Hammam Sayala hot spring case study (NW Tunisia). *Journal of African Earth Sciences*, **134**, (2017), 292–298. https://doi.org/10.1016/j.jafrearsci.2017.07.003

Dakhnov, V. N.: Geophysical well logging. *Q. Colorado Sch. Mines*, (1962), 57–2, 445.

Duba, A., J. Piwinskii, A., Santor, M., & C. Weed, H.: The electrical conductivity of sandstone, limestone and granite. *Geophysical Journal of the Royal Astronomical Society*, **53**, (1978), 583–597. https://doi.org/10.1111/j.1365-246X.1978.tb03761.x

Espinoza, A.: Estadística multivariante y geotermometría multicomponente de las manifestaciones termales del área de Pucón – Liquiñe, IX, Región de la Araucanía y XIV Región de los Ríos, Chile. Universidad de Chile. (2017).

Fikos, I., Vargemezis, G., Zlotnicki, J., R. Puertollano, J., B. Alanis, P., C. Pigtain, R.: Electrical resistivity tomography study of Taal Volcano hydrothermal system, Philippines. *Bulletin of Volcanology*, **74**, (2012), https://doi.org/10.1007/s00445-012-0638-5

Friedman, S.: Soil properties influencing apparent electrical conductivity: a review. *Computers and Electronics in Agriculture*, **46**, (2005), 45–70. https://doi.org/10.1016/j.compag.2004.11.001

Glover, P.: Archie's law – a reappraisal: *Solid Earth*, **7**, (2016), 1157–1169. https://doi.org/10.5194/se-7-1157-2016

Jubaedah, E., Bambang, T. P., & Abdurrachim.: Study of Geothermal Utilization for Milk Pasteurization in Pangalengen, Indonesia. *Proceedings*, World Geothermal Congress 2015, Melbourne, Australia (2015).

Kostoglou, M., Chrysafis, N., & Andritsos, N.: Modeling a Tomato Dehydration Process Using Geothermal Energy. *Proceedings,* World Geothermal Congress 2010, Bali, Indonesia (2010).

Loke, M.: Tutorial: 2-D and 3-D Electrical Imaging Surveys. (2004).

Lund, J., & Falls, K.: Milk pasteurization with geothermal energy. *G.H.C. Bulletin*, (1997).

Moreno, H., and Luis Lara.: Geología Del Área Liquiñe-Neltume, Regiones de La Araucanía y de Los Lagos. *Servicio Nacional de Geología y Minería, Carta Geológica de Chile, Serie Geología Básica*, **83**, (2004), 23p., 1 Mapa Escala 1:100.000,".

Perez-Flores, P., Cembrano, J., Sánchez, P., Veloso, E., Arancibia, G., & Roquer, T.: Tectonics, magmatism and paleo-fluid distribution in a strike-slip setting: Insights from the northern termination of the Liquiñe-Ofqui fault System, Chile. *Tectonophysics*, **680**, (2016), https://doi.org/10.1016/j.tecto.2016.05.016

Rees, S.: Advances in Ground Source Heat Pump Systems. WoodHead Publishing (Elsevier). (2016) https://doi.org/10.1016/C2014-0-03840-3

Revil, A., Cuttler, S., Karaoulis, M., Zhou, J., Raynolds, B., & Batzle, M.: The plumbing system of the Pagosa thermal Springs, Colorado: Application of geologically-constrained geophysical inversion and data fusion. *Journal of Volcanology and Geothermal Research*, **299**, (2015), https://doi.org/10.1016/j.jvolgeores.2015.04.005

Revil, A., & Jardani, A.: The Self-Potential Method: Theory and Applications in Environmental Geosciences. Cambridge University Press, UK. (2013). https://doi.org/10.1017/CBO9781139094252

Richards, K., Revil, A., Jardani, A., Henderson, F., Batzle, M., & Haas, A.: Pattern of shallow ground water flow at Mount Princeton Hot Springs, Colorado, using geoelectrical methods. *Journal of Volcanology and Geothermal Research*, **198**. https://doi.org/10.1016/j.jvolgeores.2010.09.001

Sánchez, P., Perez-Flores P., Arancibia, G., Cembrano, J., and Reich, M.: Crustal Deformation Effects on the Chemical Evolution of Geothermal Systems: The Intra-Arc Liquiñe-Ofqui Fault System, Southern Andes. *International Geology Review,* **55**, (2013), https://doi.org/10.1080/00206814.2013.775731.

Shah, P. H., & Singh, D.: Generalized Archie's Law for Estimation of Soil Electrical Conductivity. *Journal of Astm International*, **2**, (2005), https://doi.org/10.1520/JAI13087

Tardani, D., Reich, M., Roulleau, E., Takahata, N., Sano, Y., Perez-Flores, P.: Exploring the structural controls on helium, nitrogen and carbon isotope signatures in hydrothermal fluids along an intra-arc fault system. *Geochimica et Cosmochimica Acta*, **184**, (2016), 193–211. https://doi.org/10.1016/j.gca.2016.04.031

Telford, W. M., Geldart, L. P., & Sheriff, R. E.: Applied Geophysics. Cambridge University Press, UK, (1990). https://doi.org/10.1180/minmag.1982.046.341.32

Thayer, G., Altseimer, J., & Oscar, M.: The Demonstration Geothermal Food Dehydration Facility at Zunil, Guatamala. *Canadian Institute of Food Science and Technology Journal*, **22**, (1989), https://doi.org/10.1016/S0315-5463(89)70506-X

Tripp, A. C., Ward, S. H., Sill, W. R., M. Jr. Swift, C., & R. Petrick, W.: Electromagnetic and Schlumberger resistivity sounding in the Roosevelt Hot Springs KGRA. *Geophysics*, **43**, (1978), https://doi.org/10.1190/1.1440908

Yadav, K., & Sircar, A. (2018). Milk pasteurization by residual low enthalpy geothermal water. *Proceedings,* Grand Renewable Energy 2018 International Conference and Exhibition At: Pacifico Yokohama, Japan (2018).